Supplementary Information

Magnetic recyclable α-Fe_2O_3-Fe_3O_4/Co_3O_4-CoO nanocomposite with dual Z-scheme charge transfer pathway for quick photo-Fenton degradation of organic pollutants

Khaled Alkanad[1], Abdo Hezam[2,3], Sujay Shekar G.C.[1], Q.A. Drmosh[4], A. L. Amrutha Kala[5], Murad. Q. A. AL-Gunaid[6] and Lokanath N.K.[1*]

[1]*Department of Studies in Physics, University of Mysore, Manasagangotri, Mysuru 570 006, India.*

[2]*Center of Materials Science and Technology, Vijnana Bhavana, University of Mysore, Manasagangotri, Mysuru 570006, India.*

[3] *Department of Physics, Faculaty of Science, Ibb University, Ibb, Yemen.*

[4]*Center of Research Excellence in Nanotechnology and Physics Department, King Fahd University of Petroleum and Minerals, Dhahran 31261, Saudi Arabia.*

[5]*Food Safety and Analytical Quality Control Laboratory, CSIR-CFTRI, Mysuru, Karnataka, India.*

[6]*Deprtment of Chemistry, Faculty of Education, Dhamar University, Dhamar, Yemen.*

*E-mail:lokanath@physics.uni-mysore.ac.in

Materials

$Fe(No_3)_3.6H_2O$ (≥98%), $CoN_2O_6.6H_2O$ (98%), commercial Fe_2O_3 (99%), commercial Co_3O_4 (99%), methyl orange, trisaminomethane, sodium hydroxide, nitric acid (69%), ethanol, sodium Azide, thiourea, silver nitrate, methanol, hydrogen peroxide (30 wt. %), potassium persulfate, potassium iodide and sodium chloride and were bought from Sigma-Aldrich, glycine (99%), starch soluble, hydrochloric acid (36.5%) were purchased from Sisco research laboratories, rhodamine B, methylene blue, bisphenol A, 4- nitrophenol, 4-chlorophenol and p-benzoquinone (BQ, 98%) were purchased from Loba Chemie. Isopropyl alcohol and L-ascorbic acid were purchased from Alfa Aesar. All chemicals have been used as obtained; deionized water was used throughout the studies.

Fabrication of α-Fe_2O_3 and α-Fe_2O_3-Fe_3O_4

α-Fe_2O_3 nanoparticle (NP) has been synthesized using a facile solution combustion approach in two steps. First step 0.15 M of $Fe(No_3)_3.6H_2O$, 20 ml deionized water and a specified quantity of glycine as fuel is used such that fuel ratio equal to 0.9 were added to 500 ml beaker and vigorously stirred for 0.5 hr at room temperature and heated on a hot dish at 350°C. 10 min later, the mixture starts boiling, foaming, and then ignited, forming dark brown powder; the second step, the formed powder was crushed and further calcinated at 500^{o}C in a muffle furnace for 1hr to develop α-Fe_2O_3 NPs, the final powder was brown in color stored in a clean container and labeled as FNP.

α-Fe_2O_3-Fe_3O_4 nanocomposite (NC) has been synthesized following only the first step of the procedure used to prepare α-Fe_2O_3; the sample was then crushed and washed thoroughly with double distilled water and ethanol to eliminate the unreacted Fe and any surface residual impurities. The obtained substance was allowed to dry overnight in a hot air oven at 60^{o}C. The final product is labeled as FNC for further studies and characterizations.

Fabrication of Co_3O_4 and Co_3O_4-CoO

Co_3O_4 and Co_3O_4-CoO have been synthesized using the same procedure of synthesizing α-Fe_2O_3 and α-Fe_2O_3-Fe_3O_4, respectively, by changing the nitrate to $CoN_2O_6.6H_2O$. The obtained powder was black in color and light in weight, kept in a clean container, and labeled as CNP and CNC.

Fabrication of α-Fe_2O_3-Fe_3O_4/Co_3O_4-CoO

α-Fe_2O_3-Fe_3O_4/Co_3O_4-CoO NCs were synthesized using the same method. Typically, 0.15 M of $Fe(No_3)_3.6H_2O$ is liquefied in 80 ml deionized water, and 0.15 M of $Co(No_3)_3.6H_2O$ is liquefied in 7 ml deionized water in separate beakers and an appropriate quantity of glycine as fuel such that fuel ratio equal to 0.9 was added to each beaker. Different volumes of $Fe(No_3)_3.6H_2O$ (19.5, 19, 18, 17 ml) separated in four beakers mixed with different quantity of $Co(No_3)_3.6H_2O$ (0.5, 1, 2 and 3 ml) applied to each beaker respectively such that, the molar ratio of Fe to Co 97.5:2.5, 95:5, 90:10 , and 85:15, and labeled as F-CNCs-2.5% F-CNCs-5%, F-CNCs-10% and F-CNCs-15% respectively. Each suspension was shaken for 0.5 h and heated at 350 °C on a hot dish. After evaporation, the suspension began to boil, foam, and then ignite. The obtained powders

were getting darker with an increase in the ratio of Co. All samples were systematically cleaned with distilled water and ethanol to eliminate any residual impurities on the surface and dried overnight in a hot air oven at 60 ^{o}C. The obtained products were stored for further studies and characterizations.

Characterizations of catalysts

The crystal structures were detected by X-ray powder diffractometer (XRPD, Rigaku diffractometer, Cu Kα radiation, λ = 1.54059 Å), size stepping 0.02°, with 2θ range from 10 to 60°. Dynamic light scattering (DLS) Microtrac particle analyzer was used to detect the particle size of the catalysts. The morphology of the synthesized samples was studied using scanning electron microscopy (SEM-Hitachi-3400N) and high-resolution transmission electron microscope (HRTEM-FEI TITAN3TM). Elemental analysis was carried out using elemental mapping attached to the SEM imaging. X-ray photoelectron spectroscopy (XPS, PHI 5000 Versa Probe III) spectra of the samples were recorded from 200 to 820 eV, and the HR-XPS spectra were fitted using Gaussian function. Raman spectra were detected in the wavenumber range of 150 to 750 cm^{-1} by Raman Confocal Microscope (WITec alpha 300RA). Photoluminescence (PL) spectra were captured by a Perkin- Elmer LS55 fluorescence spectrometer. The band gap was determined by a Perkin- Elmer Lamda-34 spectrophotometer UV-visible diffuse reflectance spectroscopy (DRS UV-vis) Electron spin resonance (ESR)-trapping test was performed using the Bruker spectrometer (EMX plus model). Liquid chromatography-mass spectrometry (ESI/APCI-Hybrid Quadrupole, Time- of –flight, LCMSMS) was performed to investigate the degradation products of MO. Inductively coupled plasma optical emission spectrometry (ICP-OES) was used to measure the cobalt and iron ions leaching.

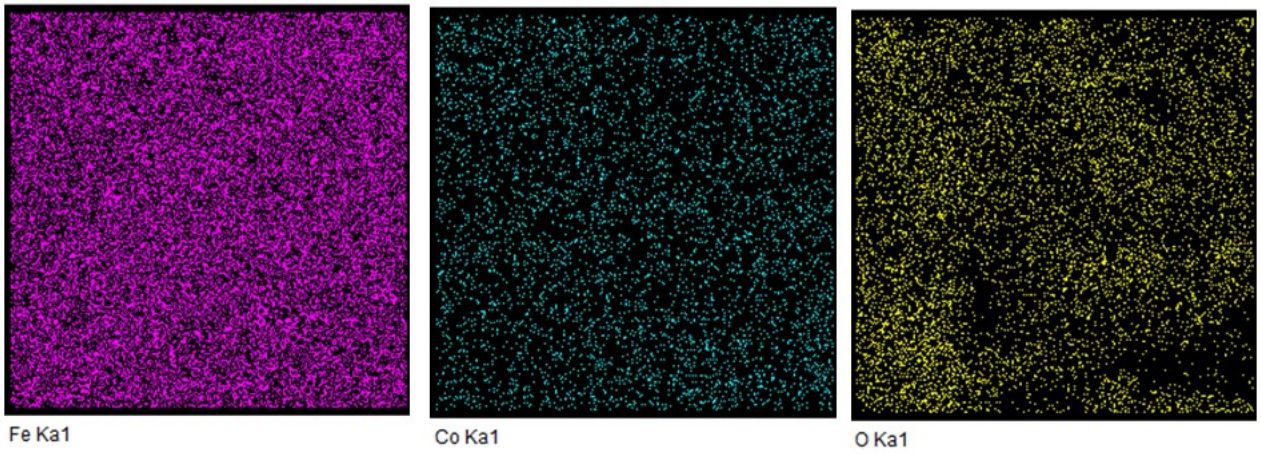

Fig.S1. Elemental mapping for FCNC-10% sample

Table S1. Slopes of -ln(C/C_0) against time of the prepared samples for the photodegradation of MO, RhB, and MB by sunlight irradiation

Sample	MO		RhB		MB	
	k	R^2	K	R^2	k	R^2
F-CNCs-10%	0.06623	0.98692	0.0639	0.90136	0.05326	0.95169
F-CNCs-5%	0.05598	0.99693	0.04464	0.98769	0.04643	0.96679
F-CNCs-15%	0.04965	0.99591	0.03987	0.96733	0.03892	0.97953
F-CNCs-2.5%	0.04529	0.99352	0.03445	0.98863	0.03513	0.97991
FNC	0.02749	0.98964	0.02368	0.99559	0.02212	0.99724
CNC	0.01297	0.98795	0.01179	0.9989	0.01022	0.99195
FNP	0.00503	0.99461	0.00359	0.9507	0.003	0.95997
CNP	0.00299	0.99549	0.00243	0.98536	0.00249	0.99149

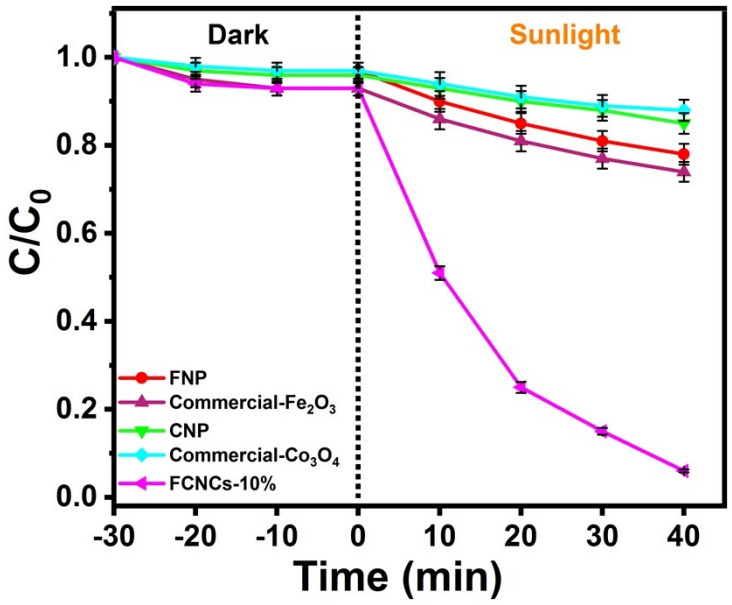

Fig. S2. Photodegradation comparison of commercial-Fe_2O_3 and Co_3O_4 with FNP, CNP, and F-CNCs-10% (1 g L^{-1} catalyst does, 10 mg L^{-1} of MO, *pH* 2.8, 85k lux sunlight intensity)

Influences of photocatalyst dosage

The influence of the photocatalyst amount on the degradation of MO has been studied by repeating the photodegradation experiment with different concentrations of F-CNCs-10% sample (from 0.4 to 2.4 g L^{-1}). The outcomes can be seen in Fig. S3. The degradation efficiency increases to a maximum of 94% with an increase in the photocatalyst dose to 2 g L^{-1} due to sufficient consumption of the photocatalyst particles in the illumination area [1]. Further, increase the amount of the photocatalyst beyond 2 g L^{-1} decreases the pollutant degradation performance due to the light scattering by photocatalyst particles [1], implying the optimum photocatalyst dose to be 2 g L^{-1}. However, there is no such decrease in the degradation efficiency after the optimum, which might be attributed to the Fenton reaction. It is worth mentioning that there is no significant difference in the photocatalytic efficiency between 1 g L^{-1} and 2 g L^{-1} dose. Therefore, all the photocatalytic studies were carried out at 1 g L^{-1}.

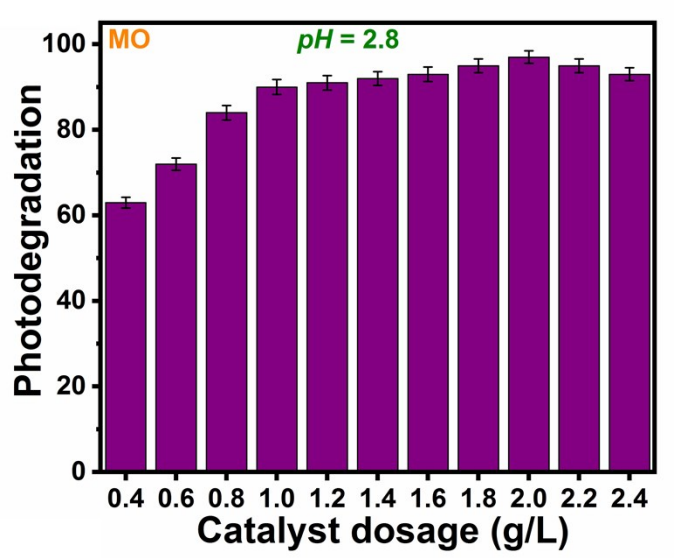

Fig. S3. Photocatalyst dosage effect of F-CNCs-10% (1 g L^{-1}), MO (10 mg L^{-1}), *p*H 2.8

***p*H studies**

*p*H plays a vital role in the Fenton processes. The optimum *p*H for the Fenton process is around three, independent of the substrate [2, 3]. To clarify the role of Fenton reaction, MO, RhB, and MB photodegradation over F-CNCs-10% were carried out at different *p*H levels. The results for all the respective dyes did not show much variation. Fig. S4 displays the results for the MO removal over F-CNCs-10% in the absence of H_2O_2. The highest degradation was achieved at *p*H 2.8, and increasing the *p*H significantly decreased dye degradation. Hence, the major degradation might be due to photocatalysis because at higher *p*H the Fenton reagent is reduced, and the oxidation potential of hydroxyl radicals decreases with increasing *p*H [2, 4]. Furthermore, increasing the *p*H beyond 6, the photodegradation decreases extensively. It was observed that at *p*H 8 and beyond, the degradation totally quashed. On the other hand, the photolysis showed slightly higher degradation than the suspension due to the light scattering and reflections (Fig. S4). At *p*H < 2.8, the photolysis shows considerable photodegradation; in addition, the photo-Fenton reaction decreases as the iron complex species react slowly at *p*H less than three [3, 5].

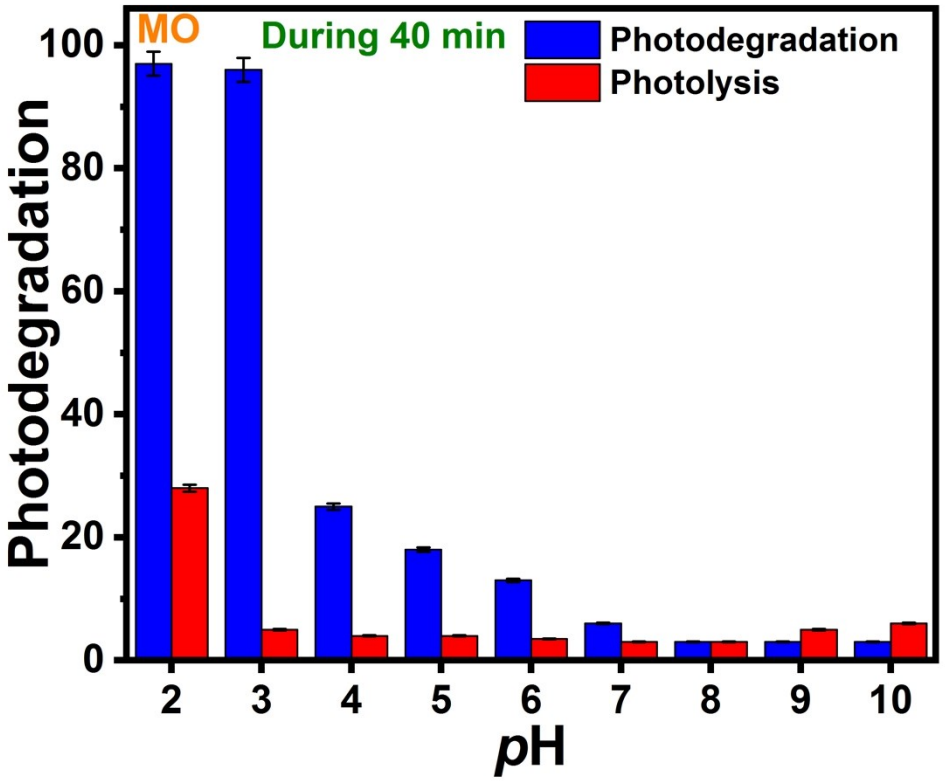

Fig. S4. Effect of different *p*H on the degradation of MO (10 mg L^{-1}) by F-CNCs-10% (1 g L^{-1})

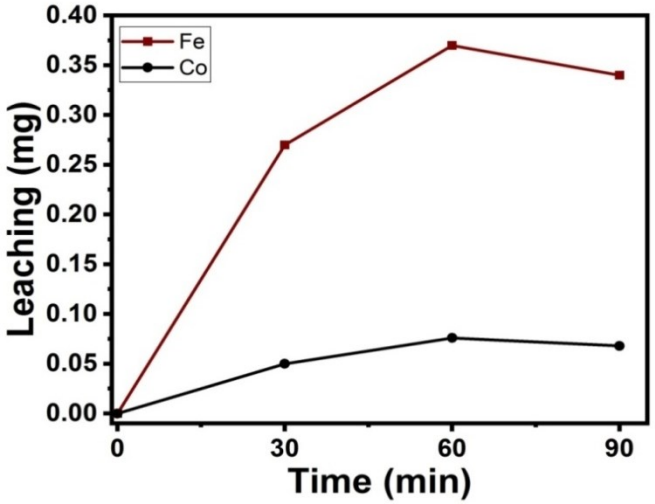

Fig. S5. The concentration of leached Fe and Co ions with time for F-CNCs-10% (catalyst does 1 g L^{-1}, MO 10 g L^{-1} *p*H = 2.8)

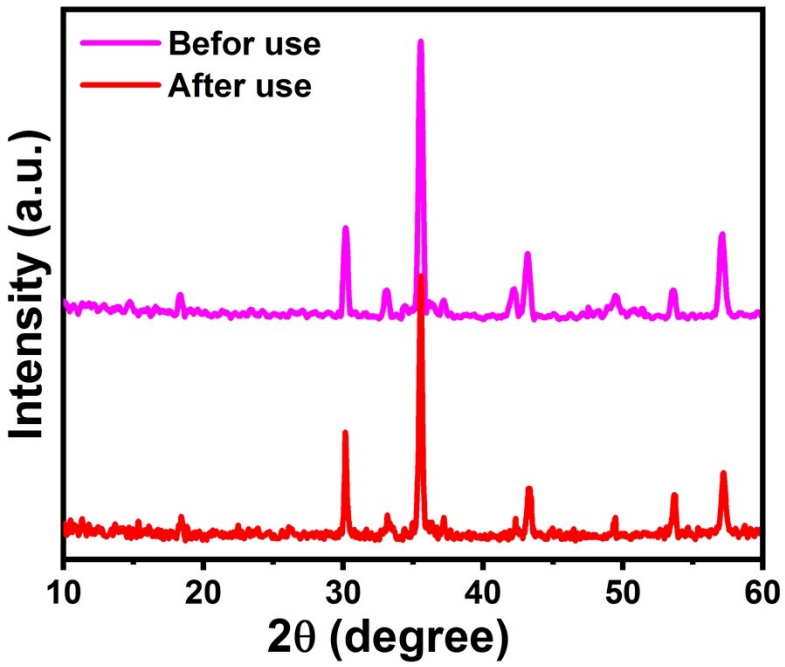

Fig. S6. XRPD patterns of FCNCs-10% photocatalyst before and after five repeated cycles

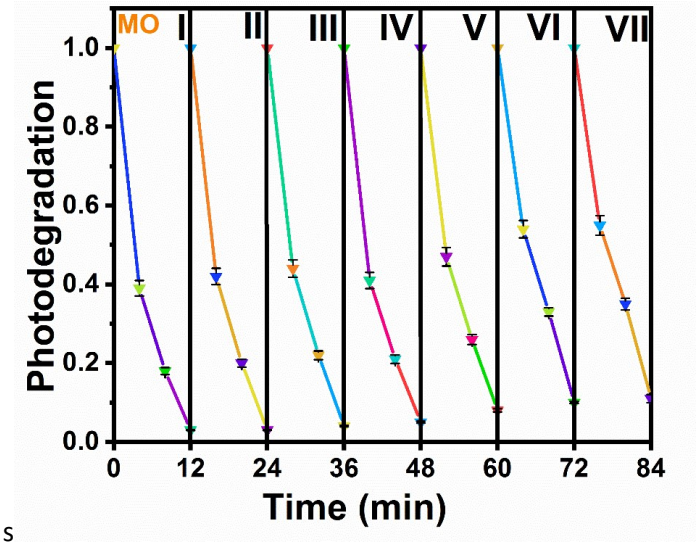

S

Fig. S7. Stability after 7 successive cycles of F-CNCs-10% (1 g L^{-1}), MO (10 mg L^{-1}), *p*H 2.8, H_2O_2 (1 mM), and 85k lux sunlight intensity

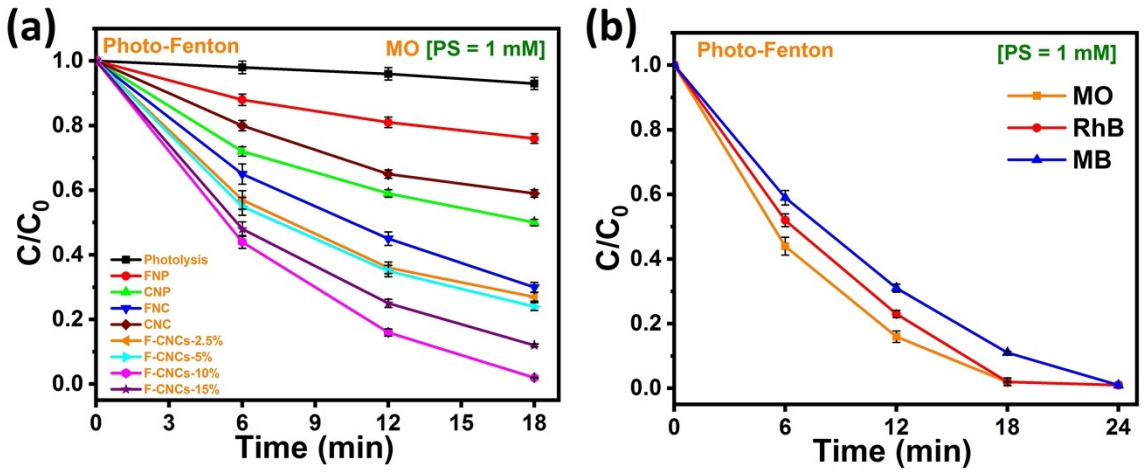

Fig. S8. PS activation as photo-Fenton degradation of (a) MO for all the samples (b) MO, RhB, and MB for F-CNCs-10% (1 g L^{-1}), dyes (10 mg L^{-1}), and *p*H 2.8

We have carried out the photodegradation in a PS system with different *p*H levels. The *p*H effect in the activated hydrogen persulfate system is shown in Fig. S9. The highest degradation was achieved at *p*H 3, and increasing the *p*H decreased the dye degradation. However, the degradation effect with different *p*H levels in the activated hydrogen persulfate system is similar to the above study (normal system (Fig. S4)).

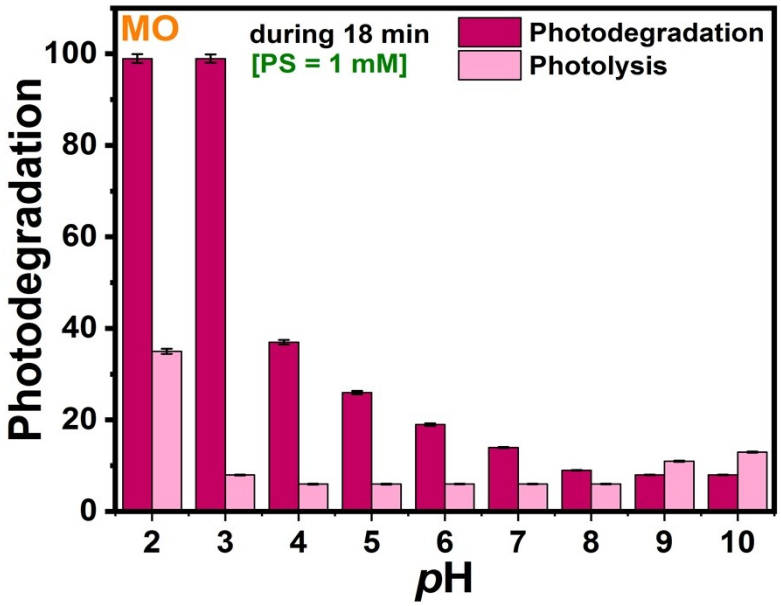

Fig. S9. MO (10 mg L^{-1}) degradation with various *p*H in the activated hydrogen persulfate system (1 mM) by F-CNCs-10% (1 g L^{-1})

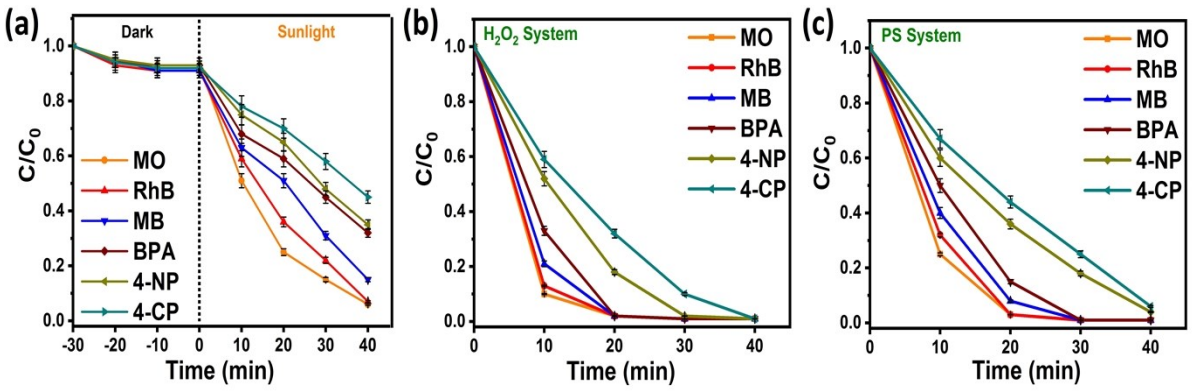

Fig. S10. (a) Degradation performance of F-CNCs-10% on different pollutants, catalyst dosage (1 g L^{-1}), pollutant concentration (10 mg L^{-1}), *p*H 2.8, and 85k lux sunlight intensity; Photodegradation at same conditions in the presence of 1 mM of (b) H_2O_2 (c) PS activators

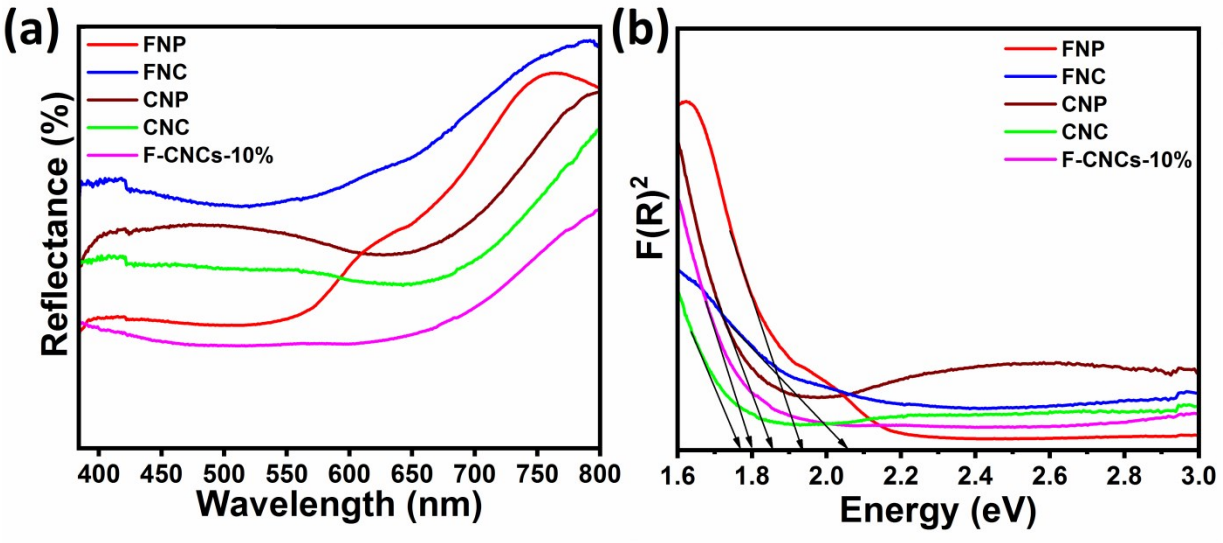

Fig. S11 (a) UV−Vis reflectance spectra, (b) Energy band gaps of FNP, FNC, CNP, CNC, and F-CNCs-10% samples

Table S2. Electronegativity, band gap, valence band maximum (VBM), and conduction band minimum (CBM) of α-Fe_2O_3, Fe_3O_4, Co_3O_4, CoO

catalyst	χ	E_g	VBM	CBM
α-Fe_2O_3	5.88	1.94	2.35	0.41
Fe_3O_4	5.78	0.1	1.33	1.23
Co_3O_4	5.908	1.85	2.328	0.47
CoO	5.23	2.43	1.95	-0.48

H_2O_2 experiment detection:

The experiment for determining the generated H_2O_2 in F-CNCs-10% suspensions was performed in glass vial aqueous suspensions of F-CNCs-10% (1 g L^{-1}) under solar light irradiation. The suspension was shaken for 30 min in the dark and then exposed to the sunlight for 40 min. The particles were removed from the suspensions by a magnet followed by filtration. 10 ml of filtrate was added to a 50 mL glass flask, and then 0.4 mL of hydrochloric acid solution (3.6 %), 1 mL of sodium chloride solution (3.4 M), 0.4 mL of soluble starch solution (30 mM), and 0.6 mL of KI solution (60 mM) were wisely dropped into the glass flask, slowly the volume of the flask was raised with water up to 20 mL. The absorbance at 582 nm of the final solution was detected by the Shimadzu UV-2450 spectrophotometer.

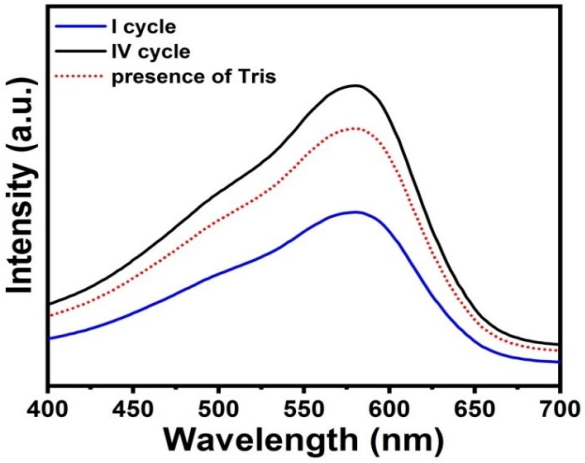

Fig. S12. In situ H_2O_2 generation in the suspension of F-CNCs-10% sample

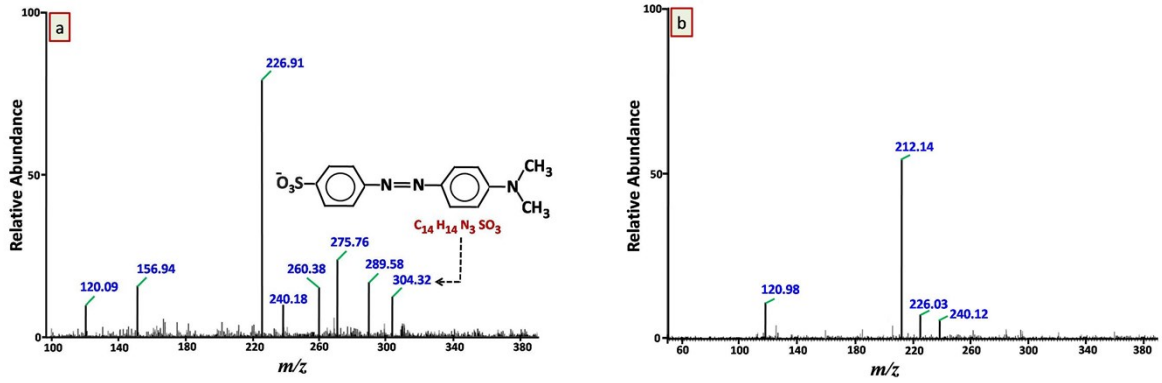

Fig. S13. Mass spectra of (a) Stock MO (10 mg L^{-1}), (b) MO after 12 min photodegradation under sunlight by F-CNCs-10% (1 g L^{-1}) with (1 mM H_2O_2 *p*H = 2.8)

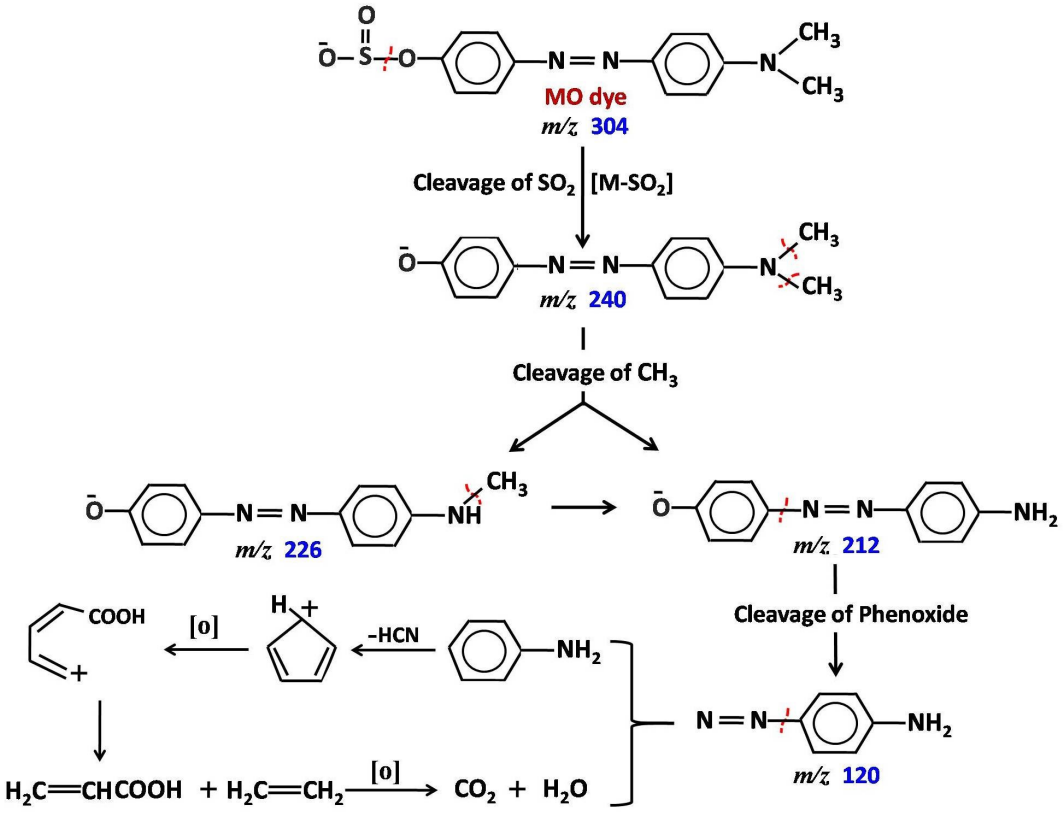

Fig. S14. Illustration of the proposed pathway for MO photodegradation in the existence FCNCs-10%

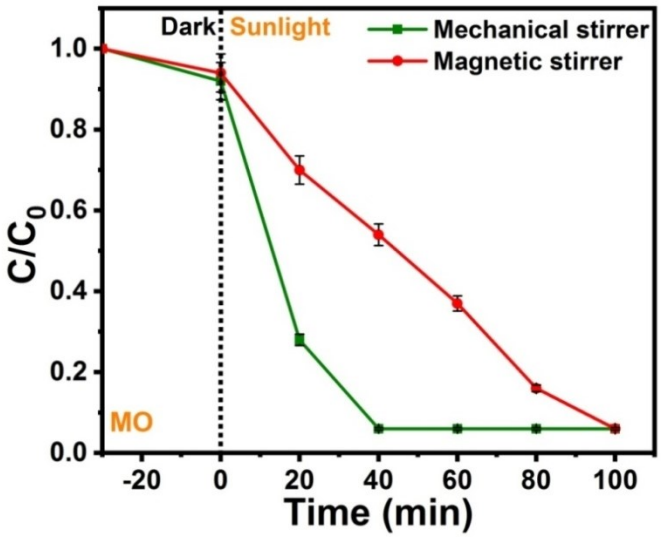

Fig. S15. Effect of the magnetic bar towards F-CNCs-10% dispersion for dye degradation

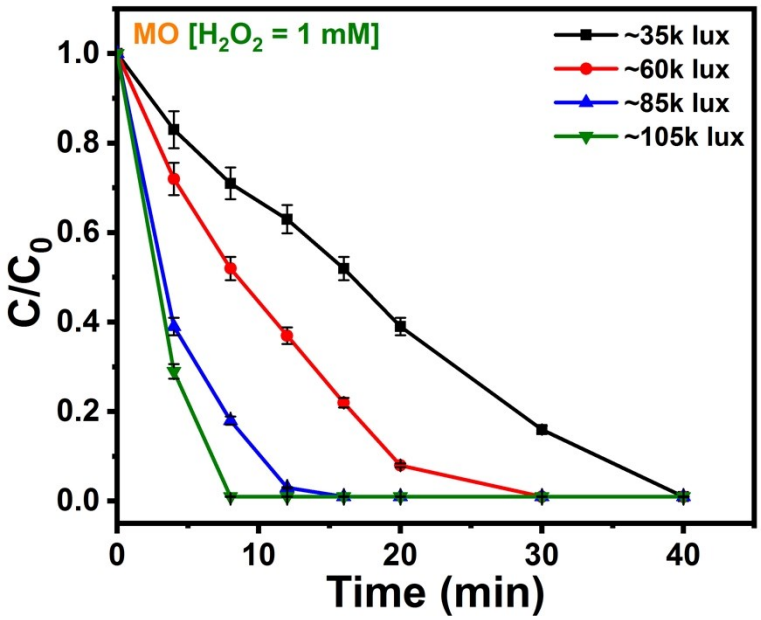

Fig. S16. Effect of solar light intensity towards MO photodegradation

References

[1] A. Hezam, K. Namratha, Q.A. Drmosh, Z.H. Yamani, and K. Byrappa, *Ceramic International*, 2017, **43**, 5292–5301.

[2] A. Babuponnusami, and K. Muthukumar, *Journal of Environmental Chemical Engineering*, 2014, **2**, 557-572.

[3] O. Primo, M.J. Rivero, and I. Ortiz, *Journal of Hazardous Material*, 2008, **153**, 834–842.

[4] S.H. Bossmann, E. Oliveros, S. Göb, S. Siegwart, E.P. Dahlen, L. Payawan, M. Straub, M. Wörner, and A.M. Braun, *Journal of Physical Chemistry A*, 1998, **102**, 5542–5550.

[5] V. Kavitha, and K. Palanivelu, *Water Resource*, 2005, **39**, 3062–3072.